

Journal Pre-proofs

Iron oxide nanospheres and nanocubes modified with carboxyphenyl porphyrin and their magnetic, optical properties and photocatalytic activities in room temperature amide synthesis

Chalathan Saengruengrit, Apoorva Sharma, Dmytro Solonenko, Patchanita Thamyongkit, Trin Saetan, Sumrit Wacharasindhu, Stefan Krause, Suchinda Sattayaporn, Georgeta Salvan, Dietrich R.T. Zahn, Numpon Insin

PII: S0304-8853(20)32482-3
DOI: <https://doi.org/10.1016/j.jmmm.2020.167515>
Reference: MAGMA 167515

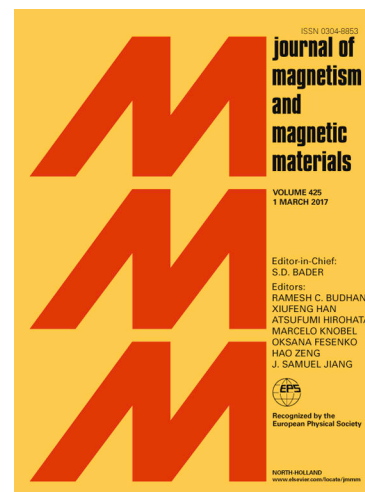
To appear in: *Journal of Magnetism and Magnetic Materials*

Received Date: 5 July 2020
Revised Date: 15 October 2020
Accepted Date: 20 October 2020

Please cite this article as: C. Saengruengrit, A. Sharma, D. Solonenko, P. Thamyongkit, T. Saetan, S. Wacharasindhu, S. Krause, S. Sattayaporn, G. Salvan, D.R.T. Zahn, N. Insin, Iron oxide nanospheres and nanocubes modified with carboxyphenyl porphyrin and their magnetic, optical properties and photocatalytic activities in room temperature amide synthesis, *Journal of Magnetism and Magnetic Materials* (2020), doi: <https://doi.org/10.1016/j.jmmm.2020.167515>

This is a PDF file of an article that has undergone enhancements after acceptance, such as the addition of a cover page and metadata, and formatting for readability, but it is not yet the definitive version of record. This version will undergo additional copyediting, typesetting and review before it is published in its final form, but we are providing this version to give early visibility of the article. Please note that, during the production process, errors may be discovered which could affect the content, and all legal disclaimers that apply to the journal pertain.

© 2020 Elsevier B.V. All rights reserved.



Iron oxide nanospheres and nanocubes modified with carboxyphenyl porphyrin and their magnetic, optical properties and photocatalytic activities in room temperature amide synthesis

Chalathan Saengruengrit^a, Apoorva Sharma^b, Dmytro Solonenko^b, Patchanita Thamyongkit^a, Trin Saetan^a, Sumrit Wacharasindhu^a, Stefan Krause^d, Suchinda Sattayaporn^c, Georgeta Salvan^b, Dietrich R.T. Zahn^b, Numpon Insin^{*a,e}

^a Department of Chemistry, Faculty of Science, Chulalongkorn University, Bangkok 10330, Thailand

^b Semiconductor Physics, Institute of Physics, Chemnitz University of Technology, 09107 Chemnitz, Germany

^c Synchrotron Light Research Institute (Public Organization), Nakhon Ratchasima, 30000, Thailand

^d Department Chemie, Ludwig-Maximilians-Universitaet Muenchen, Muenchen, Germany

^e Center of Excellence in Materials and Bio-interfaces, Chulalongkorn University, Phayathai Road, Pathumwan, Bangkok 10330 Thailand

Corresponding Author

Numpon Insin, *E-mail: Numpon.I@chula.ac.th

Abstract

Superparamagnetic iron oxide nanoparticles of different shapes and sizes combined with 5-(4-carboxyphenyl)-10,15,20-triphenylporphinatozinc(II) (SPION-ZnCTPP) were prepared and investigated as a novel and potent magnetically responsive photocatalyst. Nanospheres and

nanocubes of SPIONs in the sizes of 10 and 20 nm were synthesized using thermal decomposition method before coating with ZnCTPP. Morphologies of SPIONs were observed using a transmission electron microscope (TEM). Herein the attachment of ZnCTPP on particles was studied using various techniques including infrared spectroscopy (IR) and UV-visible spectroscopy and Inductively Coupled Plasma Optical Emission Spectroscopy (ICP-OES). Moreover, the obtained particles showed superparamagnetic character with saturation magnetization in a range of 10 to 76 emu/g, depending on the size and shape of the SPIONs. The SPION-ZnCTPP showed high photocatalytic activity (52% yield) for amide synthesis between potassium ethanethioate and 4-methoxyaniline under irradiation with a 19 W LED lamp, and this heterogeneous catalyst could be well separated from a solution under the induction of an external magnetic field.

Introduction

Recently, nanoparticles or nanomaterials have gained significant attention in many applications. Other than their unique electronic properties, as sizes of particles decreased to the nanoscale, the ratio of atoms located at the surface to atoms within the particles increases, and the resulting large surface leads to vast interaction with other molecules.[1] Due to high reactivity at the surface, chemical activities and surface modification of nanoparticles have been widely studied and utilized in various applications, including biomedicine and catalysis.[2-4] Interestingly, in many cases, the properties of nanoparticles can be tailored by controlling material compositions, sizes, shapes and their surface structures.[5]

Superparamagnetic iron oxide nanoparticles (SPION) is a class of nanomaterials which have been widely used in several applications such as drug delivery, hyperthermic cancer treatment[6], biomolecular separation, supported catalysis [7] and treatment of contaminated water[8, 9] because of their appropriate sizes and remarkable superparamagnetic character. SPIONs can be induced to exhibit strong magnetic responses using an external magnetic field and can be dispersed well in several kinds of solvents as colloid in the absence of magnetic induction.[10] SPIONs of different size and surface modification have been reported, but most of SPIONs were of spherical or irregular shapes. Monodisperse iron oxide nanocubes have been synthesized and reported to exhibit superior saturation magnetization in comparison to their

spherical counterpart. [11] However, direct comparison on surface reactivity and changes in magnetic responses of SPIONs with the same composition and similar size is still limited.

Porphyrins, organic compounds containing four pyrrole rings, exhibit interesting photochemical properties in that they have high photochemical electron transfer efficiencies and show large extinction coefficients in a visible light region.[12] Recently, organic dyes especially porphyrins have been considered to assist metal-based photocatalysts in absorbing visible light.[13] Due to advantages of porphyrin derivatives as photocatalysts, we were interested in the combination of a carboxyphenyl-substituted porphyrin derivatives with iron oxide nanoparticles via direct surface modification using its carboxylic group as an anchoring group as a model for demonstration of magnetically-responsive photocatalysts and effects of the shapes of the SPIONs on a surface modification process. Moreover, this monofunctionalized porphyrin was carefully selected to clearly observe the interaction between the SPIONs and the photocatalysts and minimize the crosslinking between the SPIONs that could interfere the surface chemistry.

Photocatalytic reactions for organic syntheses have caught many interests for their green chemistry aspect and were selected to demonstrate that the combination of SPIONs and porphyrin was achieved without the loss in their functions after the attachment of both components. We selected photocatalytic amide bond formation under room temperature as a model reaction. An amide bond is a common functional group found in many types of organic molecules, such as drug and natural products[14]; moreover, it is widely used in synthetic compounds, such as polymers and pharmaceutical products.[15, 16] However, amide synthesis methods usually involved the activation of carboxylic acid using expensive and highly hazardous coupling reagents.[17] Therefore, many catalysts have also been developed to avoid this problem, and these catalysts lead to higher efficiencies and less organic waste, but the reactions were performed in organic solvents and at high temperature.[18, 19] The photocatalyst is one of the alternative solutions for these problems, as it can activate the reaction in greener solvents at room temperature.[16] However, there is no report on the use of the porphyrin-based photocatalyst in such reaction.

In this study, the SPIONs were designed in two different shapes (nanocube and nanosphere) and two sizes (10 nm and 20 nm) for investigating their magnetic and optical

properties before and after coating with 5-(4-carboxyphenyl)-10,15,20-triphenylporphinatozinc(II) (ZnCTPP). Furthermore, the nanocomposites were preliminary tested as the catalysts for the amide synthesis under mild conditions that could be easily removed from the reaction under an external magnetic field.

Experimental

Materials and methods

Iron (III) acetylacetonate (97%), iron (III) chloride (anhydrous), oleic acid, benzyl ether (98%), and 1-octadecene were purchased from Sigma-Aldrich (MO, USA). 5-(4-carboxyphenyl)-10,15,20-triphenylporphinatozinc(II) (ZnCTPP) was synthesized according to a previous report. [20] 4-methoxyaniline (1.0 mmol) and potassium ethanethioate were purchased from TCI (Tokyo, Japan).

SPIONs preparations

SPIONs of spherical and cubic shapes with the sizes of 10 nm and 20 nm were synthesized by using a thermal decomposition method. The spherical 10 nm and 20 nm were synthesized as previously reported [21] from an iron-oleate complex as a precursor. The iron-oleate was mixed with oleic acid (stabilizer) at a mole ratio of 1:6 in 1-octadecene. Then, the resulting mixture was gradually heated to different temperatures depending on our desired size (320 °C for 10 nm and 380 °C for 20 nm SPIONs) with the rate of 3.3 °C/min). The reaction was kept at this temperature for 30 min under N₂ atmosphere. Then, the temperature was reduced to 160 °C in the air.

The synthesis of the 10-nm nanocubes were modified from previous synthesis method [22], iron oleate complex was mixed with sodium oleate and oleic in 1-octadecene. The reaction mixture was purged with nitrogen for 1 h at 150 °C and heated to 175 °C for 1 h. Then, the mixture was heated up to 320 °C with a heating rate of ~25 °C/min and maintained at this temperature for 1 h. For the synthesis of the 20-nm nanocubes [23], iron (III) acetylacetonate and oleic acid were used as the precursor and stabilizer, respectively, at various mole ratios in benzylether. The mixture of these two compounds was heated to 290 °C with the rate of 18 °C/min and maintained at this temperature for 1 h. Finally, colloidal dispersion of the magnetic nanospheres and nanocubes were

prepared in hexanes after washing for several times with a mixed solvent of 10:1 v/v ethanol-hexane.

SPION-porphyrin (SPION-ZnCTPP) preparation

10 mg SPIONs were dispersed in 300 μ L hexane, then a solution of 30 μ L ZnCTPP in THF (33 mM) was added into the SPION mixture. Subsequently, the mixture was incubated for 3 days at room temperature in the dark to prevent any possible photo-bleaching of ZnCTPP. After 3 days, the porphyrin-modified SPIONs were washed several times using ethanol and hexane in a magnetic column.

Samples Characterizations

Crystalline phases of the prepared materials were elucidated using X-ray powder diffraction (XRD) analysis (DMAX2200/Ultima-plus instrument, Rigaku, Japan), with the operation parameters of 40 kV, 30mA, Cu K-alpha radiation. Morphology and size of the SPIONs were elucidated using a transmission electron microscope (TEM) (Tecnai F20, Philips Electron Optics, Holland). The attachment of ZnCTPP onto the SPIONs was confirmed using a UV-visible spectrophotometer and a home-built confocal microscope equipped with a 405 nm UV laser (Thorlabs), an avalanche photo diode (Perkin Elmer, USA) and a liquid nitrogen cooled EMCCD camera (Princeton Instruments, USA) with spectrometer (Acton Research, USA). The ZnCTPP coating was also confirmed using Fourier-transform infrared (FT-IR) spectroscopy (Broker Vertex 80v FTIR spectrometer with a vacuum-supported sample compartment). The surface property of the nanoparticles and the nanocomposites were measured using X-ray photoelectron spectroscopy (XPS, ULVAC-PHI, Japan) with monochromatic X-ray of Al K α (1486.6 eV).

Fe₃O₄ and ZnCTPP content in nanocomposites

The Loading of Fe₃O₄ and ZnCTPP on the SPIONs and SPIONs-ZnCTPP was determined using the iron and zinc content of the particles. The sample particles were soaked in 37% hydrochloric acid for 3 h and milli-Q water was added to dilute the mixture to 5% HCl. Then, the mixture was filtrated using a 0.2 mm nylon syringe filter (VertiClean™). The iron and zinc contents were determined using an inductively coupled plasma-optical emission spectroscopy (ICP-OES, Perkin Elmer Optima 2100).

Magnetic Properties

The magnetic properties of SPIONs before and after the ZnCTPP treatment were probed using a superconducting quantum interference device - vibrating sample magnetometer (SQUID-VSM) from Quantum Design. At first, the magnetization hysteresis loops were recorded at 2K (not shown here) and at room temperature (RT). Additionally, to observe the temperature-dependent superparamagnetic-ferromagnetic transition for SPIONs and SPIONs-ZnCTPP zero-field cooled (ZFC) and field cooled (FC) measurements were performed in the temperature range of 2K to 350K in the presence of external magnetic field of 50 Oe. The standard procedure discussed elsewhere [24] was followed for the ZFC/FC measurements.

Catalytic activity of the SPION-ZnCTPP on Amide Synthesis

A Pyrex glass tube with a magnetic stirring bar was charged with 4-methoxyaniline (1.0 mmol), potassium ethanethioate (1.1 mmol), and the catalysts (1.5 μ mol of ZnCTPP) in 5 mL of 9:1 v/v ethanol and water and placed in an LED light reactor (Philips Daylight LED high Lumen 19W). The reaction mixture was stirred at room temperature for 16 h under LED irradiation. The magnetic nanocomposite catalyst was removed using magnetic separation before the mixture was filtered, and the residue was purified by chromatography with SiliaFlash G60, silica gel (70–230 mesh), (using hexane/ethyl acetate system). The product (N-(4-methoxyphenyl) acetamide) was identified using ^1H -nuclear magnetic resonance (NMR) spectroscopy (JEOL JNM-ECZ500R/S1, Tokyo, Japan). The ^1H -NMR spectrum is calibrated with chloroform peak (δ 7.26) ^1H -NMR (500 MHz, CDCl_3) δ 8.11 (s, 1H), 7.40 – 7.34 (m, 2H), 6.83 – 6.77 (m, 2H), 3.75 (s, 3H), 2.09 (s, 3H).; The ^{13}C NMR spectrum is calibrated with chloroform peak (δ 77.2) ^{13}C NMR (126 MHz, CDCl_3) δ 169.02, 156.44, 131.23, 122.23, 114.09, 55.52, 24.18.

Results and discussion

Characterization of particles

The obtained SPIONs in with different morphologies were observed using TEM (Figure 1). The spherical shapes (MS) with an average diameter of 9.5 ± 0.9 nm and 23.6 ± 1.7 nm as shown in Figures 1A and 1B were called MS10 and MS20, respectively. For the obtained magnetic nanocubes (MC) with average side length of 9.6 ± 0.8 nm and 20.4 ± 1.5 nm (Figures 1C and 1D) were denoted as MC10 and MC20, respectively.

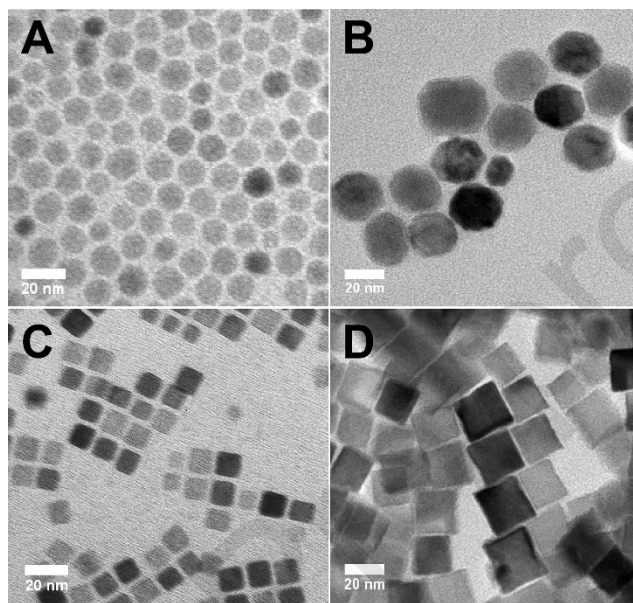


Figure 1 TEM images of SPIONs with spherical shapes: **(A)** MS10 and **(B)** MS20 and cubic shape **(C)** MC10 and **(D)** MC20.

The crystal structures of the as-synthesized particles were measured using XRD (Figure 2). XRD patterns of every sample matched with Fe_3O_4 (magnetite, JCPDS 19-0629). These well-matched patterns confirmed that the resulted nanoparticles were in ferrimagnetic phases. [25] Moreover, the XRD patterns of the larger particles (20 nm diameter) of both spherical and cubic shapes exhibited the full width at half-maximum (FWHM) of a prominent peak (35°), which was clearly sharper than that of 10 nm of sizes. This trend agreed well with the values determined using the Debye–Scherrer equation (1) at the λ of 0.154 nm ($\text{Cu K}\alpha$). [26, 27]

$$D = \frac{k\lambda}{\beta \cos \theta}$$

(1)

where k is a constant for a given instrument alignment (0.9), and β is FWHM (Full Width Half Maximum) of the peak with maximum intensity (2θ at $\sim 35^\circ$) in radians. As calculated using Equation (1), the crystal sizes of particles were 4.7, 6.4, 14.7 and 16.2 nm for MC10, MS10, MC20 and MS20, respectively. The calculated sizes were smaller than the sizes observed using TEM; however, both revealed a similar trend.

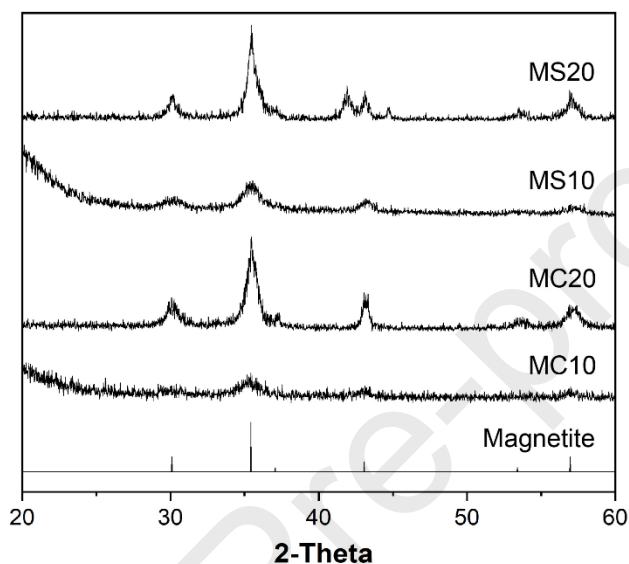


Figure 2 XRD patterns of all different shapes and sizes of SPIONs comparing with JCPDS of magnetite (Fe_3O_4 , JCPDS 19-0629).

The SPIONs containing oleic acid as stabilizer (SPION-OA) were modified with ZnCTPP to obtain the ZnCTPP-decorating SPIONs (SPION-ZnCTPP) as shown in a scheme in Figure S1. To identify the presence of ZnCTPP in the nanocomposites, we firstly used UV-vis spectroscopy to observe the spectra of SPIONs-ZnCTPP comparing with pure ZnCTPP (Figure 3). The spectrum of pure ZnCTPP showed a Soret band at 424 nm and two Q bands at 553 and 591 nm of a typical metalloporphyrin as mentioned in previous reports. [28, 29] The absorption spectra of SPIONs-ZnCTPP were also observed to be similar to that of free ZnCTPP.

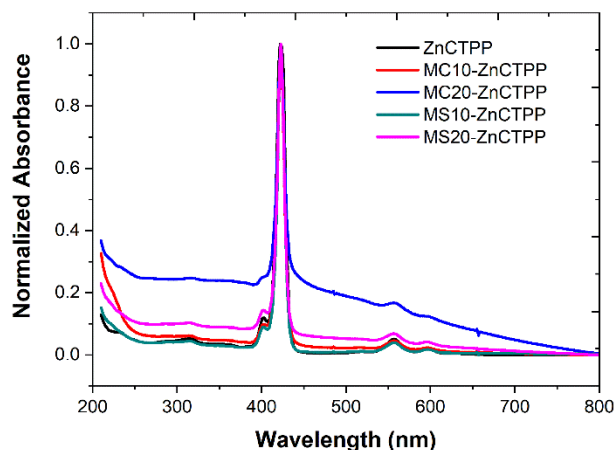


Figure 3 UV-Visible spectra of ZnCTPP-coated SPIONs of difference shapes and sizes.

Moreover, we chose two different types of the nanocomposites (MS10-ZnCTPP and MC20-ZnCTPP) to compare their fluorescence microscopic images and fluorescent spectra with free ZnCTPP (Figure 4A) and the pristine SPIONs at an excitation wavelength of 405 nm (Figures S2A and B). Figure 4A showed the fluorescence signal of pure ZnCTPP with the emission maximum at 650 nm. In a similar manner, MS10-ZnCTPP and MC20-ZnCTPP obviously displayed emission of photon and showed similar spectra to ZnCTPP (Figures 4B and 4C). These results supported the presence of ZnCTPP in the nanocomposites with maintaining optical character.

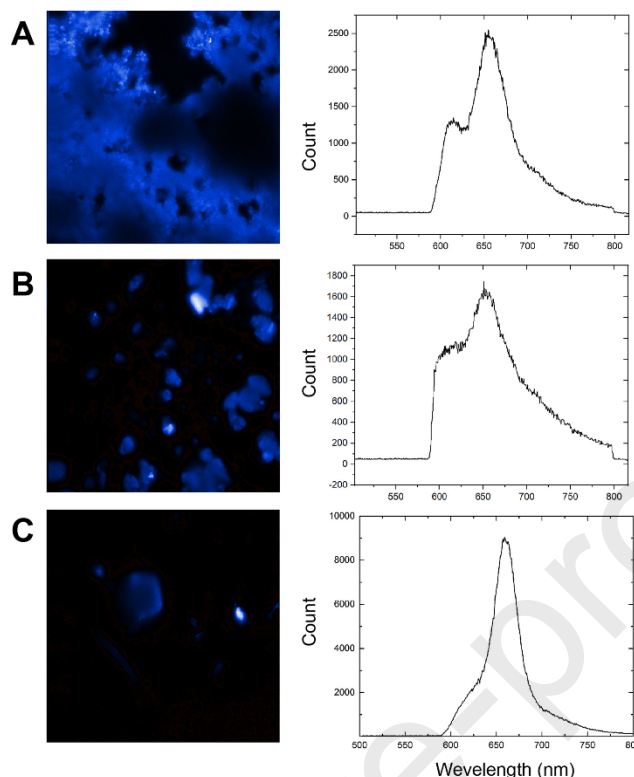


Figure 4 Confocal fluorescence images (left) and fluorescence spectra (right) of ZnCTPP (**A**), MS10-ZnCTPP (**B**) and MC20-ZnCTPP (**C**) upon excitation at 405 nm. The steep edge at around 590 nm results from the applied long pass filter.

To understand the interaction between SPIONs and the ZnCTPP, IR spectroscopy was used. Normalized IR spectra of ZnCTPP, and ZnCTPP coated SPIONs with different shapes and sizes are shown in Figure 4. IR spectra of ZnCTPP exhibited carboxyl region with the main band of C=O stretching around 1690 cm^{-1} and symmetric stretches of COO^- at around 1400 cm^{-1} . On contrary the antisymmetric COO^- appeared around $1560 - 1620\text{ cm}^{-1}$ likely due to interaction between ZnCTPP and SPIONs. Moreover, the in-plane C-N deformation mode within the porphyrin cycle demonstrated a weaker band in the region between 996 and 1005 cm^{-1} and out-of-plane C-H deformation mode at around 702 cm^{-1} . [30] Moreover, the particles showed the peak at $2950-2850\text{ cm}^{-1}$ corresponding to a C-H stretching of both oleic acid and ZnCTPP [31]. However, oleic acid was the main contribution of C-H stretching (Figure S3A), while carboxylate were more prominently observed after ZnCTPP modification (Figure S3B). After the coated onto SPIONs, the C=O stretching peaks were not observed, while the positions of COO^- stretching were slightly shifted

comparing to the unattached ZnCTPP. Therefore, ZnCTPP molecules were successfully chemisorbed on magnetic composites likely through the formation of COO^- of ZnCTPP on the SPIONs. Moreover, SPIONs-ZnCTPP showed a prominent peak at $\sim 584.3 \text{ cm}^{-1}$ that is attributed to the Fe-O bond vibration of Fe_3O_4 [32]. The unobservable Fe-O bond in MC10-ZnCTPP was probably because the large content of the oleic acid and ZnCTPP on their surface concealed the Fe-O bond, or the iron surface is partially converted to $\gamma\text{-Fe}_2\text{O}_3$ (weak band at 692 cm^{-1}). [33] All SPION-ZnCTPP showed C-H stretching of oleic acid coating on iron oxide surface at $2950 - 2850 \text{ cm}^{-1}$. [34]

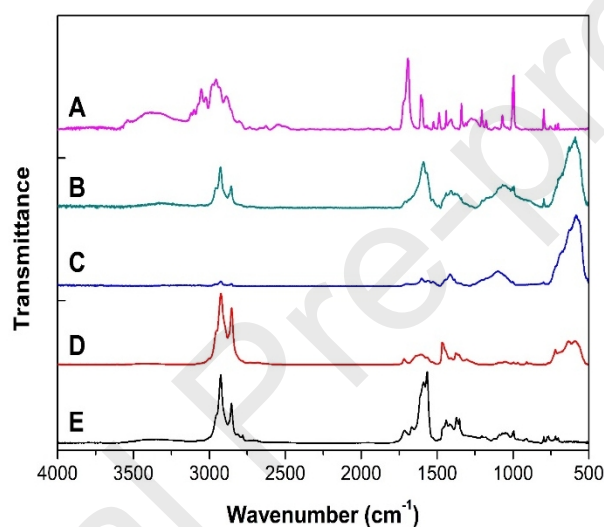


Figure 5 IR spectra of ZnCTPP (A), and the modified SPIONs with ZnCTPP: MS20-ZnCTPP (B), MC20-ZnCTPP (C), MS10-ZnCTPP (D) and MC10-ZnCTPP (E).

To further investigation on the interaction between ZnCTPP and SPION surface, XPS, a surface-sensitive technique that can detect the electronic structure of atoms within 5 to 10 nm of sample surface, was employed. [35] The technique was used to determine the zinc and iron atoms in SPIONs-ZnCTPP (Figure 6). Figure 6A exhibits the peaks corresponding to electron binding energies of $\text{Fe}2p_{3/2}$ and $\text{Fe}2p_{1/2}$ located at 711 eV and 725 eV. These peaks were associated with Fe^{3+} and Fe^{2+} species as shown in Figure 6B, confirming the formation of the Fe_3O_4 phase. [36, 37] When comparing the SPIONs and their nanocomposites, no significant changes in the binding energy of Fe, indicating that Fe played a less important role in the strong binding interaction between SPIONs and CTPP. In addition, the nanocomposites show two characteristic peaks of Zn

2p (Figure 6C and D), the spectra of pure ZnCTPP indicates the binding energies of Zn 2p_{3/2} located at 1,022 eV and Zn 2p_{1/2} at 1,045 eV.[38] All SPION-ZnCTPP samples also reveal two peaks of Zn 2p; however, the peaks were found to slightly shift towards higher energy. The shift of binding energy of Zn2p_{3/2} possibly appears because of the additional interaction of ZnCTPP with the SPIONs.

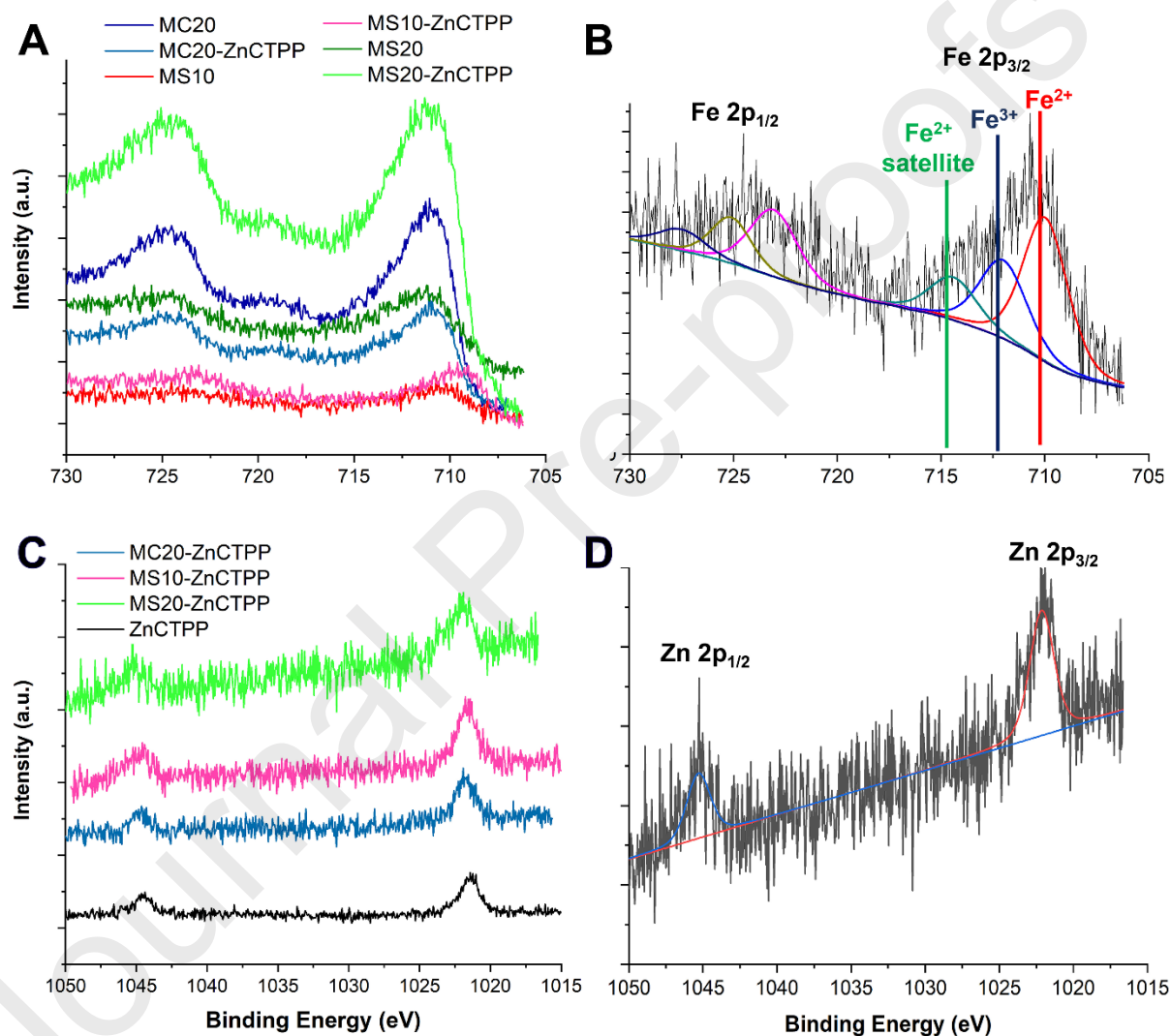


Figure 6 XPS spectra of Fe in SPIONs and SPIONs modified with ZnCTPP **(A)**, Fe 2p XPS region of nanoparticles **(B)**, XPS spectra of Zn in SPIONs-ZnCTPP comparing with ZnCTPP **(C)** and Zn 2p XPS region of the sample **(D)**.

Fe₃O₄ and ZnCTPP content in nanocomposites

Fe_3O_4 and ZnCTPP content in the nanocomposites were calculated from Fe contents as revealed by ICP-OES analysis (Table 1). Fe_3O_4 content in SPION samples of 11.0%, 82.3%, 17.6% and 84.4% were found for MC10, MC20, MS10 and MS20, respectively, indicating that the sizes played more important role than the shapes in the extension of coordination with surfactants. After coating with ZnCTPP, the Fe_3O_4 content in almost all particles tended to increase, particularly in the smaller sized particles that possessed excess oleic acid on their surface. The increasing of iron content could likely be due to the release of oleic acid from SPION surface during the surface modification. Only MC20-ZnCTPP seemed to have a slightly reduced iron content in the nanocomposite and showed the highest ZnCTPP content. However, the large content of oleic acid remained on iron surface, particularly for the small particles, as the prominent peaks of oleic acid was detected in IR spectra. Moreover, for SPIONs of our study, the ZnCTPP content of the nanocomposites was not significantly affected by the shape and size of the SPIONs, suggesting that the equilibrium between as-synthesized oleic acid and the incoming ZnCTPP was not affected by the surface area and the surface structure of the particles.

Table 1 Percentage of Fe_3O_4 and ZnCTPP in SPIONs and Fe_3O_4 in SPIONs-ZnCTPP calculated from the iron or zinc content obtained from ICP-OES analysis of the digested particles

SPIONs		SPIONs-ZnCTPP		
Samples	% Fe_3O_4	Samples	% Fe_3O_4	% ZnCTPP
MC10	11.0	MC10-ZnCTPP	24.3	2.42
MC20	82.3	MC20-ZnCTPP	78.8	3.05
MS10	17.6	MS10-ZnCTPP	22.4	2.48
MS20	84.4	MS20-ZnCTPP	87.7	2.53

Magnetic Property

Room temperature recorded magnetization hysteresis loops of the investigated SPIONs and SPIONs-ZnCTPP is shown in Figure 7. The MS10, MC10, MS20 and MC20 showed saturation magnetization (M_s) of 12.5, 18.5, 44.8 and 76.6 emu/g (emu per weight of the obtained materials).

The superparamagnetic behavior was confirmed by the absence of the coercivity in the hysteresis curves for the smaller size nanoparticles and by the narrow hysteresis loops detected for the larger nanoparticles. [39] After modification with ZnCTPP, the smaller sized nanoparticles MC10-ZnCTPP and MS10-ZnCTPP exhibited slightly higher magnetization than the as-synthesized SPIONs corresponding to the increase in Fe_3O_4 content in their structure (Table 1). In contrast, SPIONs-ZnCTPP with larger sizes showed decreases in M_s from the as-synthesized particles, especially for MC20-ZnCTPP, likely due to the lower amount of Fe_3O_4 corroborated with the fact that the attached ZnCTPP might increase the interparticle distances. From these observations, we found that even though as-synthesized iron oxide nanocubes showed higher saturation magnetization than the spherical nanoparticles of the similar size, the porphyrin-modified SPIONs exhibit the opposite trend. This might be related to larger surface area. Moreover, the magnetic measurement results confirm that the composition of the composites is highly sensitive to the surface modification process. The smaller SPIONs were stabilized by the adsorption of large quantity of excess oleic acid ligand, and these surfactants could be replaced substantially upon the surface modification process, resulting in high Fe content in the resulted nanocomposites. Interestingly, when the particles were as large as 20 nm, cubical nanoparticles exhibited higher magnetization regardless of the surface modification process.

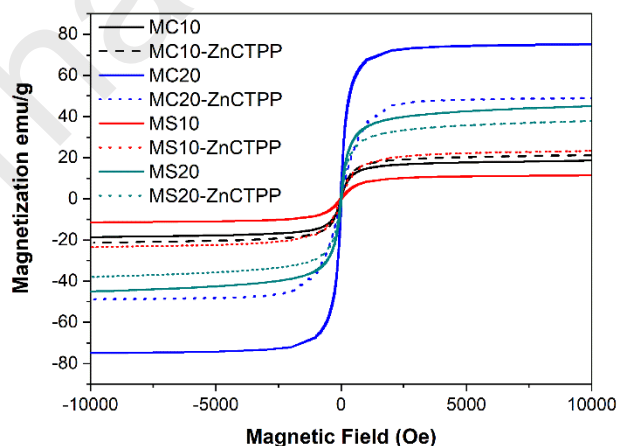


Figure 7 Magnetic properties of SPIONs compared with the nanocomposites with ZnCTPP.

Magnetic measurement applied a magnetic field at 300 K (-10000 to 10000 Oe).

Figure 8 shows the temperature dependence of the magnetization measured with ZFC and FC procedure. The SPIONs with and without ZnCTPP with the size of 10 nm (MC10, MC10-ZnCTPP, MS10, and MS10-ZnCTPP) are superparamagnetic (SPM) at room temperature (300 K), as indicated by the full convergence of the ZFC and FC curves, which bifurcate only at temperatures below 200K. Thus give the blocking temperature (T_B , the maximum of ZFC) of approximately 112 ± 9 K and 130 ± 7 K for MS10 and MC10 SPIONs, respectively.[40] Further, with the ZnCTPP treatment to MC10 and MS10 a slight increase in T_B ($T_B \sim 144\pm 10$ K) was observed. In contrast to the 10 nm SPIONs, no clear the bifurcation in ZFC/FC was observed for the SPIONs with size of 20 nm. A few subtle crests below RT can be observed in the ZFC curve for 20 nm SPIONs suggesting that these samples contain a mixture of SPIONs with several size distributions.

Firstly, we studied the temperature dependence of magnetization using standard zero field cooling (ZFC) and field cooling (FC) process (ZFC/FC) at 0 to 350 K (Figure 8). The ZFC/FC of the small size of SPIONs: MS10 and MC10 showed the characteristic feature of superparamagnetic behavior with blocking temperature (T_B , the maximum of ZFC) of approximately 112 ± 9 K and 130 ± 7 K, respectively.[41]

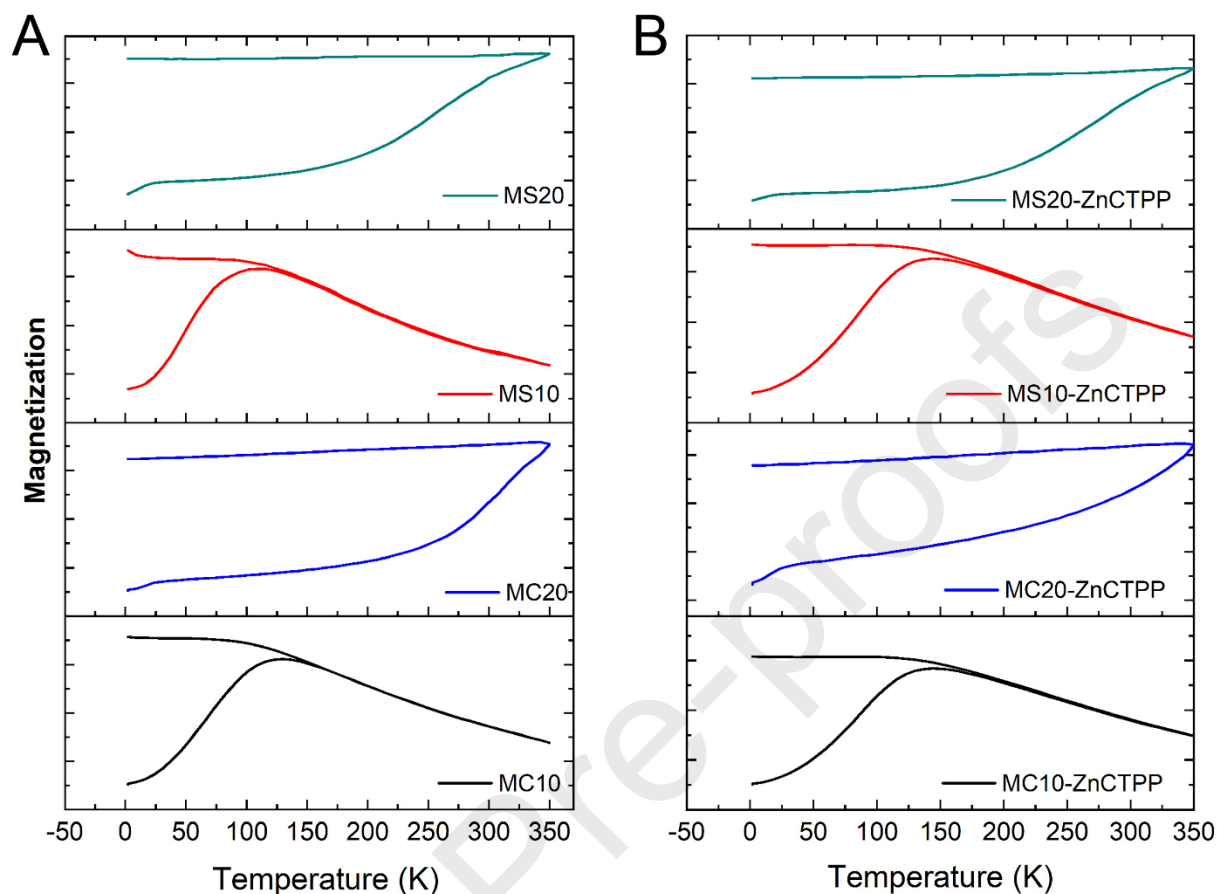


Figure 8 SQUID magnetization against temperature under field cooled (FC) and zero field cooled (ZFC) processes of SPIONs **(a)** and SPIONs-ZnCTPP **(b)** on quartz substrate for in-plane applied magnetic field at 0 K and 350 K.

Catalytic activity of the SPION-ZnCTPP on Amide Synthesis

To demonstrate that the surface modification of SPIONs with our model photocatalyst was successful without losing photocatalytic and magnetic response, the photocatalytic activity of the SPION-ZnCTPP in amide synthesis was investigated (Table 2). We selected MC20-ZnCTPP to represent the magnetic responsive photocatalyst for its highest ZnCTPP content and strongest magnetic response. In this study, potassium ethanethioate has been chosen as a representative substrate and was reacted with 4-methoxyaniline at room temperature for 16 h in mixture of water and ethanol (1:9 v/v) under white LED light irradiation. The amide coupling product was isolated by column chromatography and reported in Table 2. (Figure S3). **Free ZnCTPP was first used as a**

sole photocatalyst providing the target amide in $41.7 \pm 7.2\%$ yield. Switching the catalyst to MC20-ZnCTPP (using similar ZnMCTPP quantity (1.3 mg)), the amide product of $52.3 \pm 15.3\%$ yield was obtained. Even though the photocatalytic activity of the nanocomposites under this studied condition was not significantly different from the ZnMCTPP, the synergistic between ZnCTPP and SPIONs was expected as there were some reports of the oxidation reactions occurring in the presence of an iron compound via a free radical process. However, solely Fe_3O_4 did not show significantly catalytic activity on the reactions, and co-catalysts such as peroxides were required for the reactions to sufficiently proceeded. [17, 42]

Table 2 Catalytic activity of the ZnCTPP and MC20-ZnCTPP on amide synthesis^a

Catalyst	Catalyst Weight (mg)	Isolated Yield (%)
ZnCTPP	1.3 ± 0.3	41.7 ± 7.2
MC20-ZnCTPP	41.6 ± 1.4	52.3 ± 15.3

^aReaction condition: potassium ethanethioate (1.1 mmol), 4-methoxyaniline (1.0 mmol), in EtOH:H₂O (9:1) 5.0 mL, Isolated yields.

Conclusion

The iron oxide nanospheres of 10 and 20 nm in diameter and nanocubes of 10 and 20 nm in the side length were successfully synthesized using thermal decomposition process with controlled reaction time, temperature, and iron precursor concentration. SPIONs of different sizes and shapes were then surface modified with ZnCTPP without the change of iron oxide structure and superparamagnetic behavior. The co-existence of SPIONs-ZnCTPP after purification was observed using UV-visible absorption and fluorescent spectroscopy, while FTIR spectroscopy and XPS suggested strong interaction between ZnCTPP and SPIONs. The particles showed different M_s of 10 - 76 emu/g, with the increase in M_s for larger particles, and the nanocubes showed higher

Ms than nanosphere of the similar size. After surface modification, SPIONs-ZnCTPP exhibited the changes in *Ms* at different degree depending on the size and the shape of the SPIONs with the MC20-ZnCTPP as the highest in *Ms*. Finally, the MC20-ZnCTPP exhibited a high photocatalytic activity in amide synthesis with 52% yield in greener solvent condition at room temperature under irradiation with a LED lamp, and the particles were easily separate from solution under an induction of an external magnetic field. This study on surface modification of SPIONs with porphyrin could demonstrate the effect of shape and size of SPIONs on the magnetic response after surface modification. The novel magnetic-responsive photocatalyst show great potential of utilization and could be further developed for green amide synthesis reaction and other photocatalytic reactions in the future.

Acknowledgments

This work was financially supported by the Thailand Research Fund (MRG6280091). Saengruengrit C. was supported by Ratchadapisek Somphot Fund for Postdoctoral Fellowship, Chulalongkorn University.

Reference

- [1] R.A. Crane, T.B. Scott, Nanoscale zero-valent iron: Future prospects for an emerging water treatment technology, *J. Hazard. Mater.*, 211-212 (2012) 112-125.
- [2] N.V.S. Vallabani, S. Singh, Recent advances and future prospects of iron oxide nanoparticles in biomedicine and diagnostics, *Biotech*, 8 (2018) 279.
- [3] Y. Guo, M. Dai, Z. Zhu, Y. Chen, H. He, T. Qin, Chitosan modified Cu₂O nanoparticles with high catalytic activity for p-nitrophenol reduction, *Appl. Surf. Sci.*, 480 (2019) 601-610.
- [4] S. Li, L. Xiao, H. Deng, X. Shi, Q. Cao, Remote controlled drug release from multi-functional Fe₃O₄/GO/Chitosan microspheres fabricated by an electrospray method, *Colloids Surf. B Biointerfaces*, 151 (2017) 354-362.

- [5] O. Penon, M.J. Marín, D.B. Amabilino, D.A. Russell, L. Pérez-García, Iron oxide nanoparticles functionalized with novel hydrophobic and hydrophilic porphyrins as potential agents for photodynamic therapy, *J. Colloid Interface Sci.*, 462 (2016) 154-165.
- [6] M. Bañobre-López, A. Teijeiro, J. Rivas, Magnetic nanoparticle-based hyperthermia for cancer treatment, *Rep. Pract. Oncol. Radiother.*, 18 (2013) 397-400.
- [7] D. Kanakaraju, N.R.b.M. Shahdad, Y.-C. Lim, A. Pace, Magnetic hybrid TiO₂/Alg/FeNPs triads for the efficient removal of methylene blue from water, *Sustain. Chem. Pharm.*, 8 (2018) 50-62.
- [8] X. Zhao, J. Wang, F. Wu, T. Wang, Y. Cai, Y. Shi, G. Jiang, Removal of fluoride from aqueous media by Fe₃O₄@Al(OH)₃ magnetic nanoparticles, *J. Hazard. Mater.*, 173 (2010) 102-109.
- [9] R. Chalasani, S. Vasudevan, Cyclodextrin-Functionalized Fe₃O₄@TiO₂: Reusable, Magnetic Nanoparticles for Photocatalytic Degradation of Endocrine-Disrupting Chemicals in Water Supplies, *ACS nano*, 7 (2013) 4093-4104.
- [10] P.M. Enriquez-Navas, M.L. Garcia-Martin, Chapter 9 - Application of Inorganic Nanoparticles for Diagnosis Based on MRI, *Front. Nanosci.*, (2012) 233-245.
- [11] D. Amara, J. Grinblat, S. Margel, Solventless thermal decomposition of ferrocene as a new approach for one-step synthesis of magnetite nanocubes and nanospheres, *J. Mater. Chem.*, 22 (2012) 2188-2195.
- [12] M. Moshari, M. Rabbani, R.J.R.o.C.I. Rahimi, Synthesis of TCPP-Fe₃O₄@S/RGO and its application for purification of water, *Res. Chem. Intermed.*, 42 (2016) 5441-5455.
- [13] S. Afzal, W.A. Daoud, S.J. Langford, Photostable Self-Cleaning Cotton by a Copper(II) Porphyrin/TiO₂ Visible-Light Photocatalytic System, *ACS Appl. Mater. Interfaces*, 5 (2013) 4753-4759.

- [14] T. Cupido, J. Tulla-Puche, J. Spengler, F. Albericio, The synthesis of naturally occurring peptides and their analogs, *Curr. Opin. Drug Discov. Devel.*, 10 (2007) 768-783.
- [15] R.M. Lanigan, P. Starkov, T.D. Sheppard, Direct Synthesis of Amides from Carboxylic Acids and Amines Using $B(OCH_2CF_3)_3$, *J. Org. Chem.*, 78 (2013) 4512-4523.
- [16] S. Das, S. Ray, A.B. Ghosh, P.K. Samanta, S. Samanta, B. Adhikary, P. Biswas, Visible light driven amide synthesis in water at room temperature from Thioacid and amine using CdS nanoparticles as heterogeneous Photocatalyst, *Appl. Organomet. Chem.*, 32 (2017) 1-10.
- [17] S.C. Ghosh, J.S.Y. Ngiam, C.L.L. Chai, A.M. Seayad, T.T. Dang, A. Chen, Iron-Catalyzed Efficient Synthesis of Amides from Aldehydes and Amine Hydrochloride Salts, *Adv. Synth. Catal.*, 354 (2012) 1407-1412.
- [18] J. Franzen, A. Fisher, Asymmetric alkaloid synthesis: a one-pot organocatalytic reaction to quinolizidine derivatives, *Angew. Chem. Int. Ed. Engl.*, 48 (2009) 787-791.
- [19] D. Kundu, A. Majee, A. Hajra, Zwitterionic-type molten salt: An efficient mild organocatalyst for synthesis of 2-amidoalkyl and 2-carbamatoalkyl naphthols, *Catal. Commun.*, 11 (2010) 1157-1159.
- [20] D.H. Apaydin, H. Seelajaroen, O. Pengsakul, P. Thamyongkit, N.S. Sariciftci, J. Kunze-Liebhäuser, E. Portenkirchner, Photoelectrocatalytic Synthesis of Hydrogen Peroxide by Molecular Copper-Porphyrin Supported on Titanium Dioxide Nanotubes, *Chem. Cat. Chem.*, 10 (2018) 1793-1797.
- [21] J. Park, K. An, Y. Hwang, J.G. Park, H.J. Noh, J.Y. Kim, J.H. Park, N.M. Hwang, T. Hyeon, Ultra-large-scale syntheses of monodisperse nanocrystals, *Nat. Mater.*, 3 (2004) 891-895.

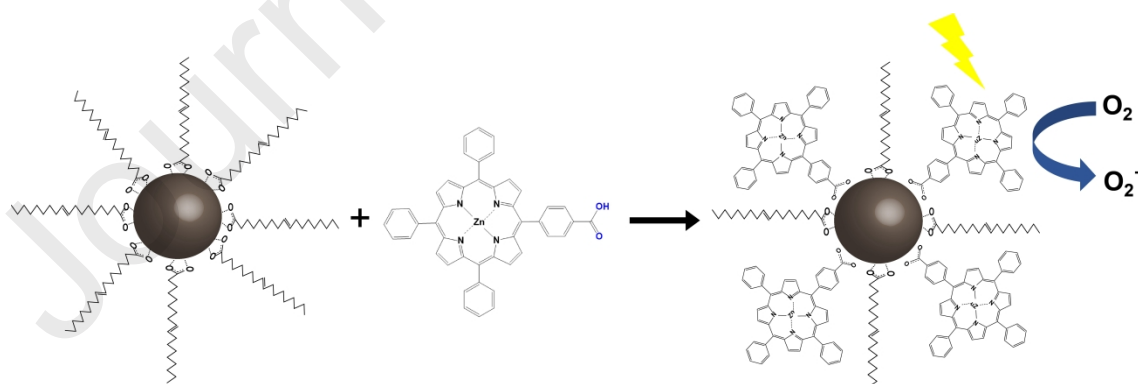
- [22] A. Shavel, L.M. Liz-Marzán, Shape control of iron oxide nanoparticles, *Physical Chemistry Chemical Physics*, 11 (2009) 3762-3766.
- [23] D. Kim, N. Lee, M. Park, B.H. Kim, K. An, T. Hyeon, Synthesis of Uniform Ferrimagnetic Magnetite Nanocubes, *Journal of the American Chemical Society*, 131 (2009) 454-455.
- [24] M.F. Hansen, S. Mørup, Estimation of blocking temperatures from ZFC/FC curves, *J. Magn. Magn. Mater.*, 203 (1999) 214-216.
- [25] Q. Liu, X. Chen, J. Jia, W. Zhang, T. Yang, L. Wang, G. Ma, pH-Responsive Poly(D,L-lactic-co-glycolic acid) Nanoparticles with Rapid Antigen Release Behavior Promote Immune Response, *ACS nano*, 9 (2015) 4925-4938.
- [26] I. Karimzadeh, M. Aghazadeh, M.R. Ganjali, P. Norouzi, S. Shirvani-Arani, T. Doroudi, P.H. Kolivand, S.A. Marashi, D. Gharailou, A novel method for preparation of bare and poly(vinylpyrrolidone) coated superparamagnetic iron oxide nanoparticles for biomedical applications, *Mater. Lett.*, 179 (2016) 5-8.
- [27] M. Asrofi, H. Abrial, A. Kasim, A. Pratoto, M. Mahardika, J.-W. Park, H.-J. Kim, Isolation of Nanocellulose from Water Hyacinth Fiber (WHF) Produced via Digester-Sonication and Its Characterization, *Fibers and Polymers*, 19 (2018) 1618-1625.
- [28] W. Zheng, N. Shan, L. Yu, X. Wang, UV-visible, fluorescence and EPR properties of porphyrins and metalloporphyrins, *Dyes and Pigments*, 77 (2008) 153-157.
- [29] M.S. Kang, J.B. Oh, S.G. Roh, M.-R. Kim, J.K. Lee, S.-H. Jin, H. K. Kim, Novel Extended π -Conjugated Dendritic Zn(II)-porphyrin Derivatives for Dye-sensitized Solar Cell Based on Solid Polymeric Electrolyte: Synthesis and Characterization, *Bull. Korean Chem. Soc.*, 28 (2007) 33-40.

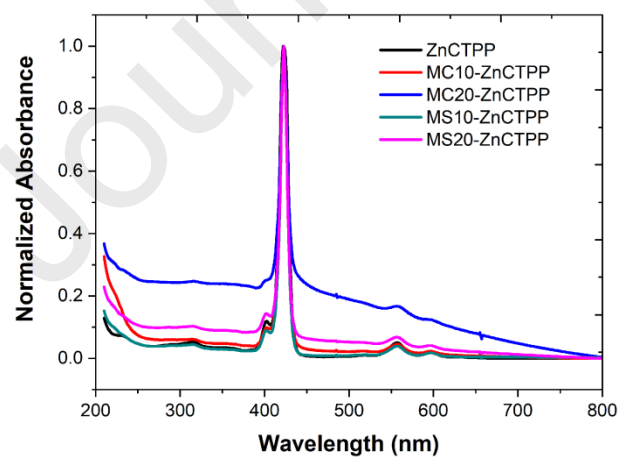
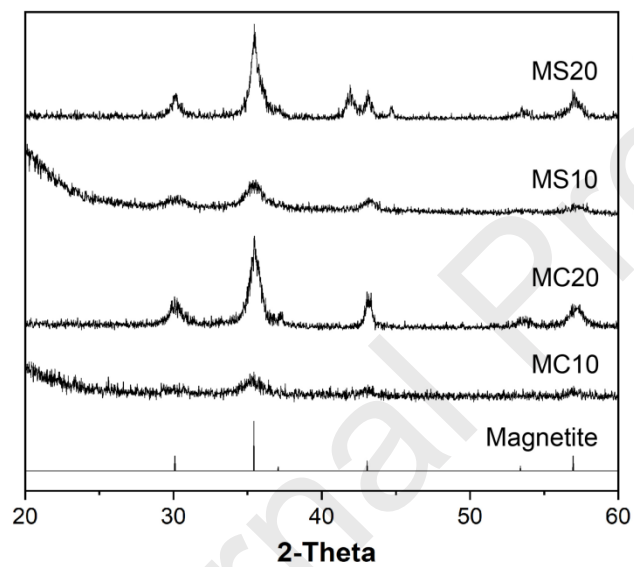
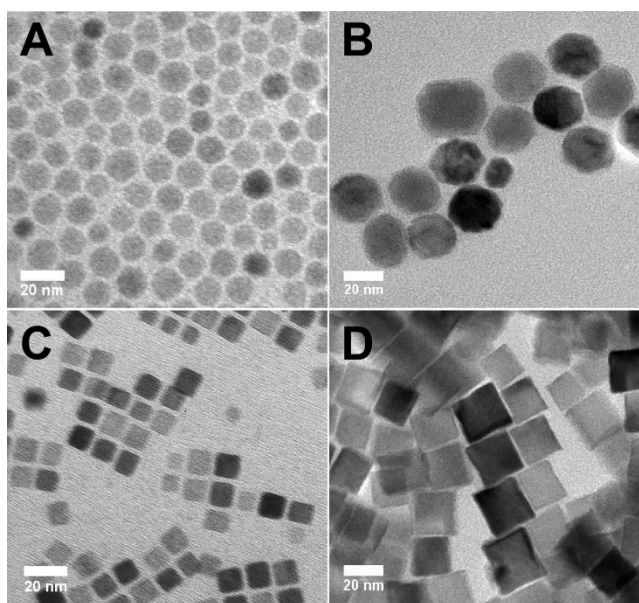
- [30] K. Werner, S. Mohr, M. Schwarz, T. Xu, M. Amende, T. Dopfer, A. Gorling, J. Libuda, Functionalized Porphyrins on an Atomically Defined Oxide Surface: Anchoring and Coverage-Dependent Reorientation of MCTPP on $\text{Co}_3\text{O}_4(111)$, *J. Phys. Chem. Lett.*, 7 (2016) 555-560.
- [31] Saengruengrit, C.; Ritprajak, P.; Wanichwecharungruang, S.; Sharma, A.; Salvan, G.; Zahn, D. R. T.; Insin, N., The combined magnetic field and iron oxide-PLGA composite particles: Effective protein antigen delivery and immune stimulation in dendritic cells. *J. Colloid Interface Sci.* 2018, 520, 101-111.
- [32] J. Sun, S. Zhou, P. Hou, Y. Yang, J. Weng, X. Li, M. Li, Synthesis and characterization of biocompatible Fe_3O_4 nanoparticles, *J. Biomed. Mater. Res.*, 80A (2007) 333-341.
- [33] Y.-S. Li, J.S. Church, A.L. Woodhead, F. Moussa, Preparation and characterization of silica coated iron oxide magnetic nano-particles, *Spectrochimica Acta Part A: Molecular and Biomolecular Spectroscopy* 76(5) (2010) 484-489.
- [34] M. Bloemen, W. Brulot, T.T. Luong, N. Geukens, A. Gils, T. Verbiest, Improved functionalization of oleic acid-coated iron oxide nanoparticles for biomedical applications, *J. Nanopart. Res.*, 14 (2012) 1100.
- [35] M.S. Wagner, Molecular depth profiling of multilayer polymer films using time-of-flight secondary ion mass spectrometry, *Anal. Chem.*, 77 (2005) 911-922.
- [36] X. Guo, B. Guo, Preparation of Fe_3O_4 -porphyrin nano-composited particles and their optical and magnetic properties, *Chem. Res. Chinese U.*, 33 (2017) 530-533.
- [37] Q. Ai, Z. Yuan, R. Huang, C. Yang, G. Jiang, J. Xiong, Z. Huang, S. Yuan, One-pot co-precipitation synthesis of Fe_3O_4 nanoparticles embedded in 3D carbonaceous matrix as anode for lithium ion batteries, *J. Mater. Sci.*, 54 (2019) 4212-4224.
- [38] D. Xu, D. Fan, W. Shen, Catalyst-free direct vapor-phase growth of $\text{Zn}_{1-x}\text{Cu}_x\text{O}$ micro-cross structures and their optical properties, *Nanoscale Res. Lett.*, 8 (2013) 46-46.

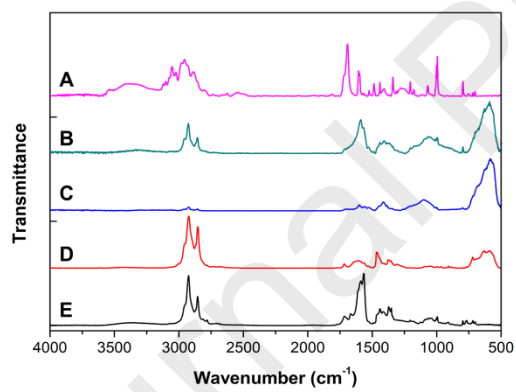
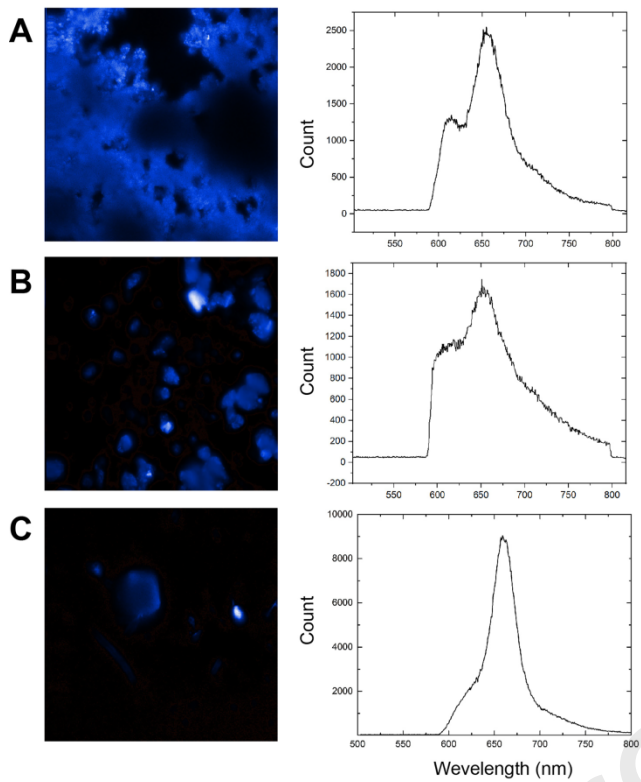
- [39] Z. Alborzi, A. Hassanzadeh, M.M. Golzan, Superparamagnetic Behavior of the Magnetic Hysteresis Loop in the Fe₂O₃@Pt Core-Shell Nanoparticles, *J. Nanosci. Nanotechnol.*, 8 (2012) 93-98.
- [40] C. Liu, B. Zou, A.J. Rondinone, Z.J. Zhang, Chemical Control of Superparamagnetic Properties of Magnesium and Cobalt Spinel Ferrite Nanoparticles through Atomic Level Magnetic Couplings, *J. Am. Chem. Soc.*, 122 (2000) 6263-6267.
- [41] A. Modwi, O.M. Lemine, M. Alshammari, A. Houas, Ferromagnetism at room temperature in Zn_{0.95}Cu_{0.05}O nanoparticles synthesized by sol-gel method, *Mater. Lett.*, 194 (2017) 98-101
- [42] W. Wu, Z. Wang, Q. Shen, Q. Liu, H. Chen, Fe-Catalyzed enaminone synthesis from ketones and amines, *Org. Biomol. Chem.*, 17 (2019) 6753-6756.

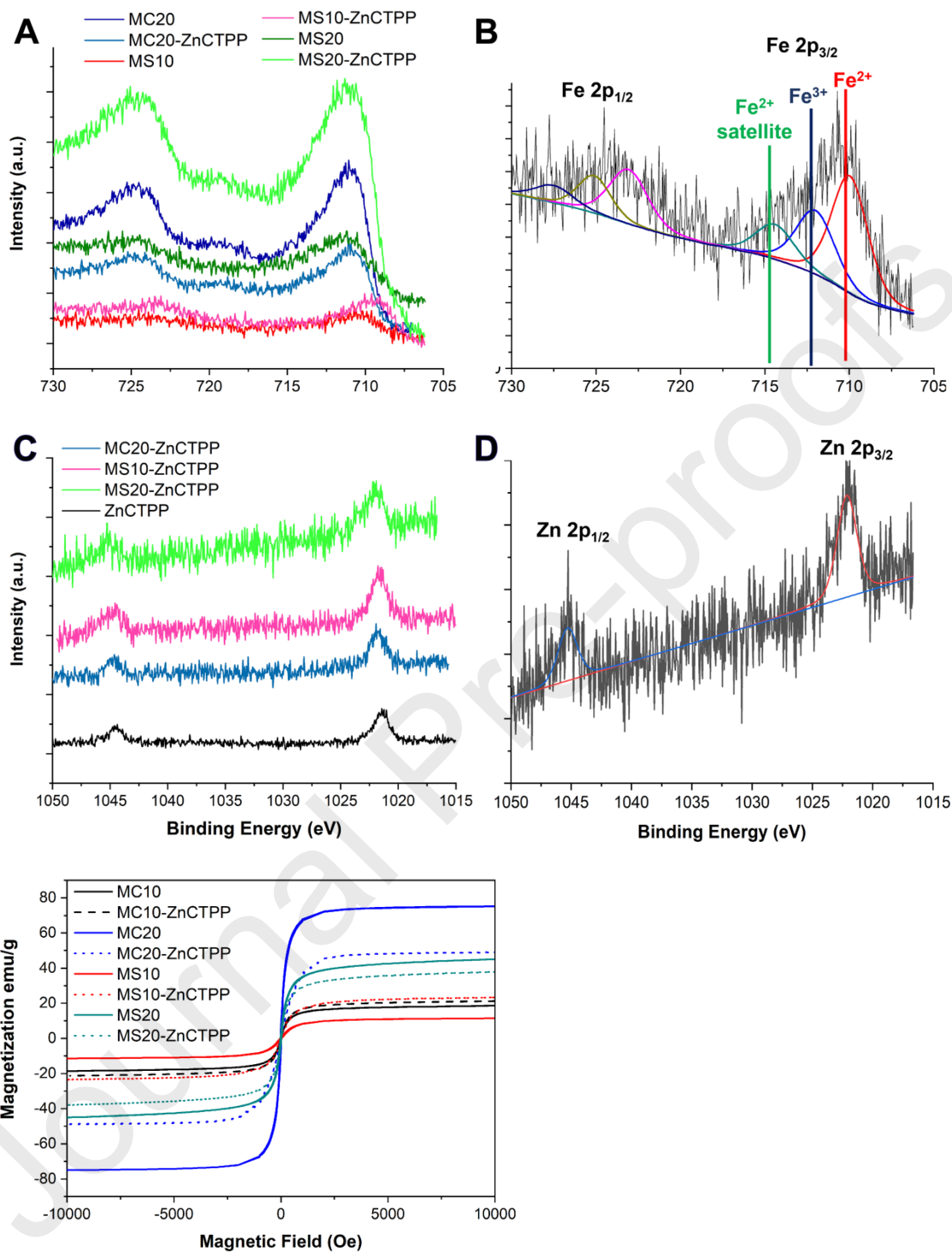
Highlights

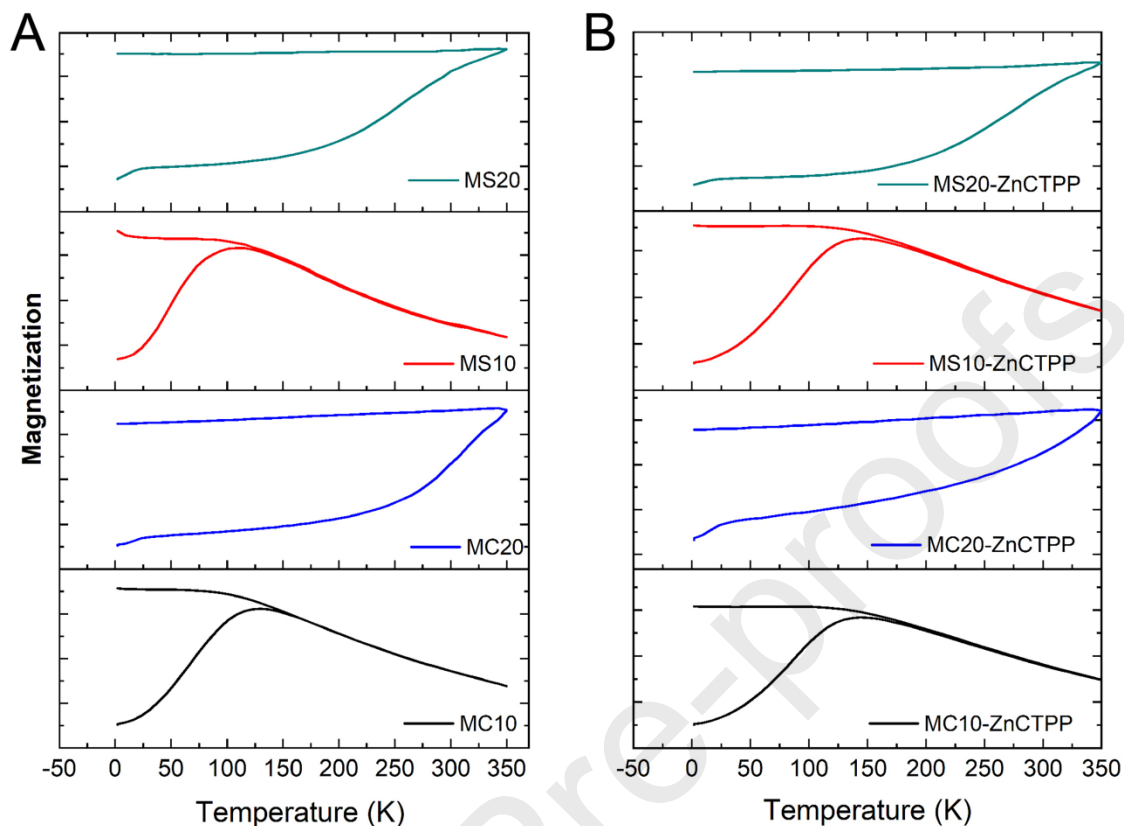
- Magnetite nanocubes and nanospheres with a carboxyphenyl porphyrin were prepared.
- Effects of size and shape of the nanostructures were discussed.
- Photocatalytic activity on amide synthesis was demonstrated at room temperature.











CRediT author statement

Chalathan Saengruengrita

Methodology, Formal analysis, Investigation, Resources, Writing - Original Draft, Writing - Review & Editing

Apoorva Sharma

Methodology, Formal analysis, Investigation, Resources, Writing - Original Draft, Writing - Review & Editing

Dmytro Solonenko

Methodology, Formal analysis, Investigation, Resources, Writing - Review & Editing

Patchanita Thamyongkit

Conceptualization, Methodology, Resources, Writing - Review & Editing, Funding acquisition

Trin Saetan

Formal analysis, Investigation, Resources

Sumrit Wacharasindhu

Methodology, Formal analysis, Resources, Writing - Review & Editing

Stefan Krause
Methodology, Formal analysis, Resources

Suchinda Sattayaporn
Resources

Georgeta Salvan
Conceptualization, Methodology, Formal analysis, Investigation, Resources, Writing
- Original Draft, Writing - Review & Editing, Supervision, Funding acquisition

Dietrich R.T. Zahn
Conceptualization, Resources, Writing - Review & Editing, Supervision, Funding
acquisition

Numpon Insin
Conceptualization, Methodology, Resources, Writing - Original Draft, Writing -
Review & Editing, Supervision, Funding acquisition